Synthesis of Pure Silica MWW Zeolite in Fluoride Medium Using an Imidazolium-Based Long Dication

Peng Lu,[ab] Luis Gómez-Hortigüela,[c] and Miguel A. Camblor*[a]

[a] Dr. P. Lu, Prof. M. A. Camblor
Instituto de Ciencia de Materiales de Madrid (ICMM), Consejo Superior de Investigaciones Científicas (CSIC), c/ Sor Juana Inés de la Cruz 3, 28049 Madrid (Spain)
E-mail: macamblor@icmm.csic.es
[b] Dr. P. Lu
Dalian National Laboratory for Clean Energy, Dalian Institute of Chemical Physics, Chinese Academy of Sciences, Zhongshan Rd.116023, Dalian (P.R. China),
[c] Dr. L. Gómez-Hortigüela
Instituto de Catálisis y Petroleoquímica (ICP), Consejo Superior de Investigaciones Científicas (CSIC), c/ Marie Curie 2, 28049 Madrid (Spain)

Abstract: As the spacer length in 1,2-dimethylimidazolium-based dications increases beyond a point (six-methylene units), they fail in structure-directing towards the STW zeolite in any synthesis condition. They can instead produce, under fluoride concentrated conditions, either *BEA (for the eight methylene unit SDA) or MWW (ten methylene units). For any length of the dication, the default zeolite (MTW) is a relatively dense zeolite containing an unidimensional channel, whereas the zeolite demanding most specificity (STW, *BEA or MWW) is more porous, affording a larger concentration of the dication to be occluded. This work provides the first reported fluoride synthesis of pure silica MWW. Charge balance of the organic dications in this zeolite is achieved by combined “structural” silanolates, regular “connectivity defects” and occluded fluoride. Molecular mechanics calculations show a perfect fit of decamethylenebis(dimethylimidazolium) dication in the sinusoidal intralayer pore system of MWW, while the dication is also able to stabilize the interlayer space without disturbing the hydrogen bonding system that holds the layers together in the as-made material. The ^{19}F MAS NMR presents two distinct resonances at -71 and -83 ppm which, on the basis of DFT calculations, we tentatively assign to fluoride occluded in [$4^6 6^2$] and [$4^1 5^2 6^2$] cages of the MWW structure, respectively. The same DFT study determines a different chemical shift of one methyl ^{13}C nuclear magnetic resonance according to the imidazolium ring residing in the sinuosidal channels or in the large cup-cavities, thus explaining an experimentally observed splitting of that resonance.

Introduction

Zeolites, micro-crystalline aluminosilicates made up of corner-shared tetrahedra, are widely used in catalysis and adsorption applications.[1] The synthesis of these useful materials is normally carried out by the hydrothermal method through a hydroxide ion mediated route. Introduction of the fluoride ion as a mineralizer was pioneered by Flanigen and Patton for the synthesis of pure silica MFI (zeolite structure types are designated by three letter codes assigned by the International Zeolite Association, IZA)[2] zeolite,[3] and later on this fluoride route has been extensively used for the synthesis of other zeolites, clathrasils and alumino- and gallo-phosphates.[4]

MWW zeolite has attracted a great interest since it was first synthesized as an aluminosilicate named PSH-3 using hexamethyleneimine (HMI) as structure-directing agent (SDA) with alkali metal and hydroxide as a mineralizer.[5] Isostructures of MWW zeolites obtained through the hydroxide route also include SSZ-25,[6] MCM-22,[7] and ERB-1.[8] The structure of MWW zeolite was elucidated by Leonowicz et al. as an unusual framework containing two sets of independent 10MR channels (one sinusoidal, the other straight) and large 12MR supercages.[7] Typically, the fully connected MWW structure is only achieved after topotactic condensation of the as-synthesized layered precursor (pMWW).[8] Its peculiar pores have made MWW an attractive candidate for catalytic applications in refinery and petrochemical processes. The first pure silica analogue of MWW zeolite was reported and given the name ITQ-1 in 1996.[9] However, the synthesis, which made use of the relatively bulky and rigid trimethyladamantamonium cation (TMAda$^+$) at high pH, was long and hard to reproduce. Later on, the smaller and more flexible hexamethyleneimine (HMI) was introduced as a co-template together with the sodium ion, and then highly reproducible results were reported, always through the hydroxide-mediated route.[10] The beneficial effect of the second organic additive was interpreted as resulting from the stabilization of the intralayer sinusoidal channel, too large to accommodate TMAda$^+$, which was assumed to fill the half 12MR supercages in the interlayer region. Subsequently, hydrocarbon sorption properties have been explored on the ITQ-1 zeolite, which showed different diffusion rates for linear and branched C6 paraffins, opening up its potential use for separation applications.[11]

For the synthesis of pure silica zeolites, the fluoride route has been proved quite applicable especially for getting “free of defects” structures, drastically contrasting to the analogues obtained through the hydroxide route.[12] Defect-free pure silica zeolites present several advantages over defective zeolites for adsorption applications, such as a strict hydrophobicity,[13] important if water may compete for adsorption, and a lack of catalytic activity that may be fundamental to avoid side-reactions, such as the polymerization of alkenes in the separation of alkenes/alkanes mixtures.[14] Although prior endeavors towards the successful syntheses of moderately high-

silica MWW zeolites in the presence of fluoride ion were reported, boron or aluminium plus alkali metals were also necessary ingredients.[15]

Here, we report the synthesis at close to neutral pH of pure silica materials using dimethylimidazolium-based long dications (nBDMI, where n denotes the number of methylene units in the spacer between dimethylimidazolium moieties). The synthesis parameters and products are shown in Scheme 1. For the shorter dications (n=4, 5, 6) we have reported previously the synthesis of the chiral STW or achiral MTW zeolites, depending both on the specific dication and/or on the synthesis conditions.[16] As the spacer length increases, structure direction towards STW loosens and for n=6, this zeolite could only crystallize in the presence of Ge. With the longer dications (n=8, 10), too large to fit the imidazolium moieties into two consecutive cavities of STW, MTW dominates the crystallization field. However, with 8BDMI it is possible to crystallize BEA* zeolite instead under very concentrated conditions, following the Villaescusa's rule.[12a, 17] More interestingly, with 10BDMI the layered precursor to zeolite MWW (pMWW) crystallized at very low water contents. To the best of our knowledge, the present study is the first example of pure silica pMWW crystallized through the fluoride route without the presence of alkali metals, boron or aluminum.

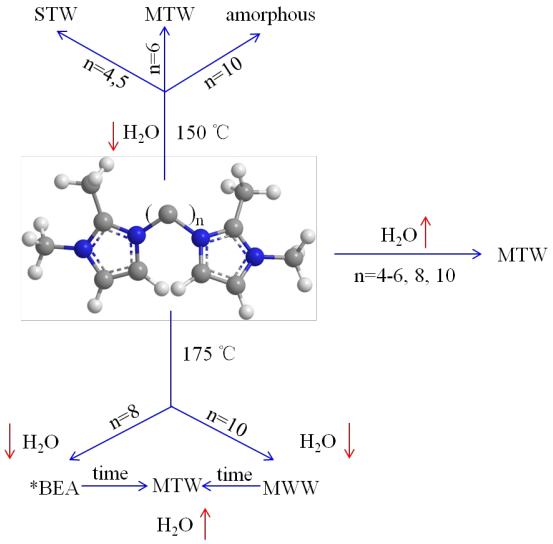

Scheme 1.Synthesis scheme of pure silica zeolites using nBDMI as SDAs.

Results and Discussion

Zeolite synthesis

The synthesis parameters and products obtained are summarized in Table 1. 10BDMI was found to be a very poor SDA at 150 °C, yielding mainly an amorphous phase and traces of an unknown phase with prolonged heating. The XRD patterns of the unknown phases formed are shown in Figure S1 and the assignation of these phases was unsuccessful due to its weak peak intensity especially at the low angle region. The rest of the experiments were then performed at 175 or 190 ºC.

By increasing the temperature to 175 °C, three crystalline phases formed quickly (Table 1) using 10BDMI. Under the most concentrated condition with water/silica ratio of 3, pure silica zeolite pMWW crystallized and coexisted with amorphous phase after heating for 24 h. Well crystallized pMWW formed with prolonged heating up to 48 h, yet MTW was always present in trace amounts (as demonstrated by the XRD patterns in Figure 1, with MTW peaks marked with *). Further increase of crystallization time to 96 h rendered pure MTW without any sign of the coexistence of pMWW, indicating a transformation process from the less dense phase (MWW, 15.9 T/1000 Å after condensation of the layered precursor) to the denser and presumably more stable one (MTW, 18.2 T/1000 Å) by Ostwald ripening. By decreasing the concentration (H_2O/SiO_2 = 4), pMWW was again obtained with some amorphous solid after short heating time (30 h). However, *BEA showed up instead of pMWW after prolonged heating to 48 h, and a mix phase of *BEA and MTW crystallized after treatment for 72 h (Figure S2). MTW formed fast under more diluted condition (H_2O/SiO_2 = 5) with a minor amount of pMWW co-existing after hydrothermal treatment for 48 h.

Table 1. Summary of the synthesis conditions and the products obtained.

SDA	Temperature (°C)	H_2O/SiO_2	time (h)	phase
10BDMI	150	3	24	amorphous
			91	amorphous
			181	amorphous(unknown)
		5	24	amorphous
			72	amorphous
			192	amorphous(unknown)
	175	3	24	pMWW+amorphous
			36	pMWW(MTW)
			42	pMWW(MTW)
			48	pMWW(MTW)
			96	MTW
		4	30	pMWW+amorphous
			48	*BEA+amorphous
			72	*BEA+MTW
		5	48	MTW(pMWW)
			120	MTW
			288	MTW
	190	3	18	MTW+pMWW
			22	MTW(pMWW)
			26.5	MTW(pMWW)
8BDMI	175	3	48	*BEA
			120	*BEA
			216	*BEA
		5	24	Amorphous
			48	MTW (*BEA)
			144	MTW
			240	MTW
			544	MTW
			504	MTW

Major phases are listed first, trace phases are included within parentheses.

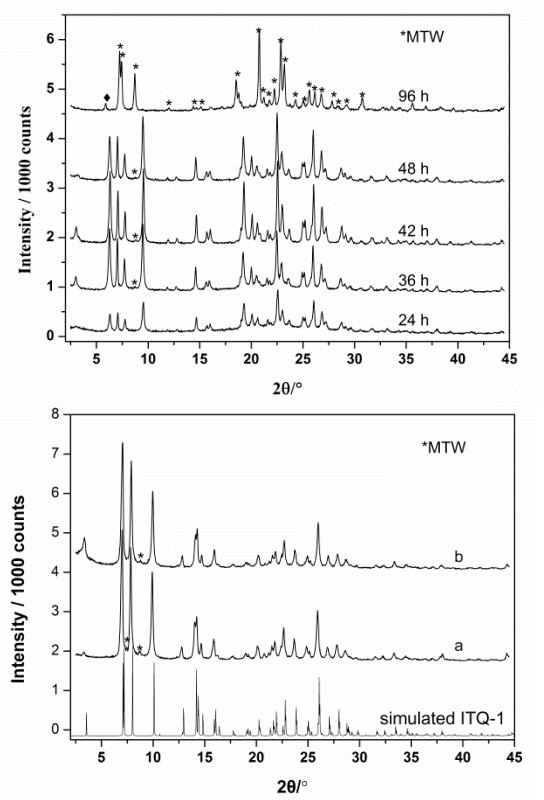

Figure 1. Powder XRD patterns of (top panel) as-made pure silica zeolites at different crystallization times under 175 °C with H_2O/SiO_2 = 3 and (bottom panel) calcined samples synthesized at (a) 42 h and (b) 48 h in comparison with simulated ITQ-1. The MTW phase is marked with "*" and the "♦" marks an extra peak of uncertain origin appearing in this particular sample.

Elevating the temperature to as high as 190 °C for the most concentrated (H_2O/SiO_2 = 3) gel made the crystallization rate faster and the "default" MTW phase was dominant. It cocrystallized with pMWW after very short heating time (18 h); after prolonging the crystallization time to 26.5 h, pMWW appeared only in trace amounts, which means, in other words, that Oswald ripening happened too fast and consequently the metastable pMWW was unfavored under such a high temperature.

In general, the crystallization of pMWW in fluoride medium using 10BDMI as the SDA was quite sensitive to the several parameters investigated. Low water/silica ratio and moderately high temperature favored the formation of pMWW in a short heating time. Higher water ratios and temperatures or prolonged heating tend to favor the denser MTW.

With regard to 8BDMI, only syntheses at 175 ºC were carried out. At a very high concentration *BEA (Figure S3) crystallized, but upon dilution only traces of this phase were observed and MTW was the dominant phase.

Characterization

The powder XRD patterns of the as-made pMWW zeolites (Figure 1, top) are well-resolved indicating the high crystallinity

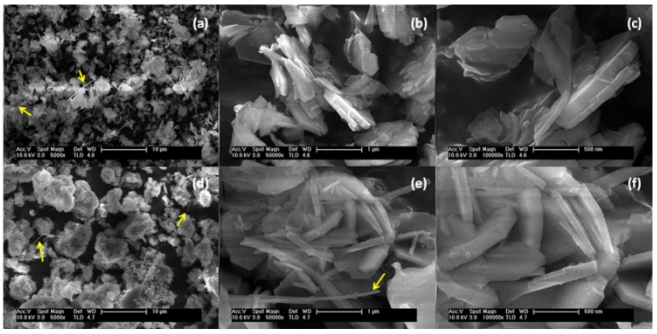

Figure 2. SEM images of as-made pMWW zeolites synthesized at 42 h (a, b, and c) and 48 h (c, d and e). Yellow arrows point to rod-like crystals likely corresponding to an MTW impurity.

of the products formed in the fluoride medium, which are more obvious for the calcined final zeolites (Figure 1, bottom). MTW, the "impurity" phase appearing in minor amount, was preserved after calcination. With regard to the as-made MTW obtained with 10BDMI, there is occasionally a small extra peak on the very left, at 5.9° (Figure 1 top, top trace), that has also been seen in some of our previous synthesis and that it is unclear if arises from a change of crystal symmetry or it is an impurity. The presence of MTW in as-made samples can be corroborated by the SEM images as shown in Figure 2. A small amount of elongated rod-like crystals can be observed in both samples (as indicated by the yellow arrows), a typical morphology of MTW zeolites (Figure 2). The dominant large flat hexagonal-shaped crystals can be assigned to the pure silica pMWW zeolite. Prolonged heating time from 42 h to 48 h rendered slightly larger crystals. In contrast to the pMWW analogues synthesized in hydroxide medium, which normally bear thin platelet-like morphology,[18] the fluoride route produced slightly thicker crystals (up to 200 nm).

The different behavior of 10BDMI at various temperatures, especially at the high temperatures of 175 and 190 °C successfully rendering MWW zeolites, might cast doubts about the integrity of the organics. High temperature may cause degradation, and the degraded organic species might have

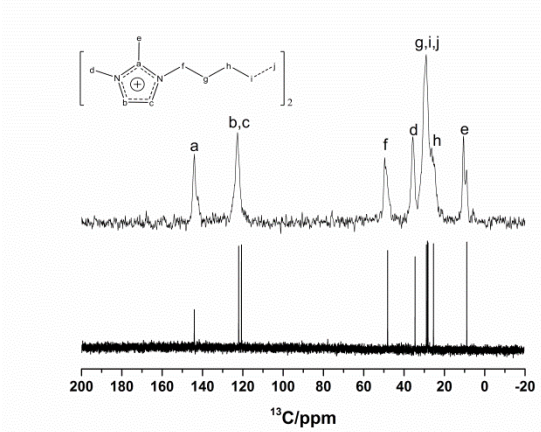

Figure 3. ^{13}C NMR spectrum in D_2O of pristine 10BDMI (bottom) and solid-state ^{13}C MAS NMR spectrum of as-made 10BDMI-MWW (top).

Table 2. Chemical composition of the as-made BEA and MWW zeolites.

phase	C(%)	H(%)	N(%)	C/N[a]	H/N[a]	TG[b]	empirical composition[c]
8BDMI-*BEA	11.8	1.97	2.78	4.95(4.5)	9.85(8.0)	80.47(82.5)	$\|C_{18}H_{32}N_4F_2\|_{2.38}[SiO_2]_{64}$:8.8 H_2O
10BDMI-MWW	14.72	2.45	3.25	5.28(5.0)	10.47(9.0)	74.17(76.2)	$\|C_{20}H_{36}N_4F_2\|_{3.19}[SiO_2]_{72}$:9.38$H_2O$

[a]Molar ratios, the theoretical values of 10BDMI are given in parentheses. [b]Solid residues (*w*%) after thermogravimetric analysis to 1000 °C (the amount in parentheses stands for the SiO_2 content in a unit cell given in the last column). [c]SDA calculated from the N percent assuming the organics are intact, and are charge-balanced by F^- ion (see text), the residue after TG is SiO_2 and the water content is derived from the excess H/N ratio (this may be due to both –SiOH and/or water).

worked as effective SDAs towards target products, as it has been reported before.[19] In this regard, it is important to know whether the organic is occluded intact in the MWW zeolite. CHN analysis of the as-made MWW was carried out and the results are shown in Table 2. C/N ratio is close to the stoichiometric expectation for 10BDMI, and the N% and TG residue suggest there are about 3 cation-like species per unit cell of the MWW framework. On the other hand, the high H/N ratio suggests the presence of water or Si-OH connectivity defects in the as-made material. However, the chemical analysis does not rule out degradation since the measured molar ratios are somewhat higher than the expected values. Hence, we performed ^{13}C MAS NMR on the as-made material, as shown in Figure 3 (top). The spectrum shows resonances close to the expected ranges for each C atom, confirming the integrity of the organic dication.

However, a splitting was observed for carbon e, which corresponds to the methyl group bonded to the imidazolium ring at position 2. This splitting could be due to different locations, orientations and/or conformations of the imidazolium rings of 10BDMI, and this will be studied below in the computational section.

Figure S4 shows the TG and DTG analysis of the pure silica MWW precursor. A minor weight loss of about 1.5% below 150 °C indicates the elimination of loosely bound water from the precursor material. The weight loss in the range of 250 to 1000 °C was due to the removal of the occluded 10BDMI, which can be divided into three stages: the combustion of 10BDMI in the inter-layer spaces in the low temperature region of 250 to 400 °C accounting for the largest amount of weight loss; the removal of 10BDMI occluded in the intra-layers of 10MR sinusoidal channels occurring in the region of 400 to 500 °C; and finally a broad DTG curve in the region of 500 to 700 °C assigned to the combustion of the coke formed during the temperature elevation process.[20] Based on the TG-DTG data, the weight loss of the as-made pure silica MWW precursor is mainly contributed by the incorporated 10BDMI molecules with a weight percentage of 24.4% based on the weight loss region above 150 °C, which is larger than the amount (20.4%) determined by the sum of C, H and N elemental analysis. The difference is likely due to the elimination of F anions and dehydroxilation of silanols (see below).

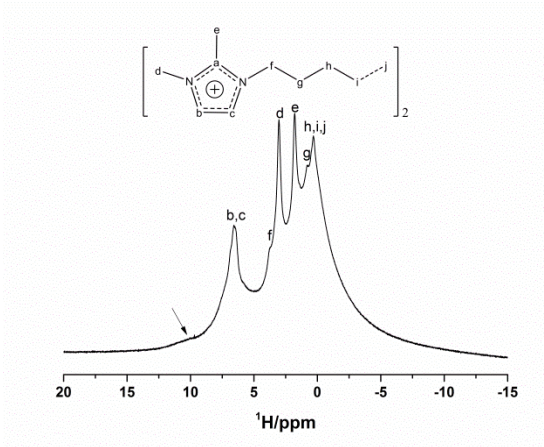

Figure 4. ^1H MAS NMR spectrum of as-made 10BDMI-MWW. The a-j letters refer to H assignments to the C labelled in the dication. A broad band marked with an arrow at 10 ppm is assigned to SiOH hydrogen bonded to charge compensating SiO^- groups.

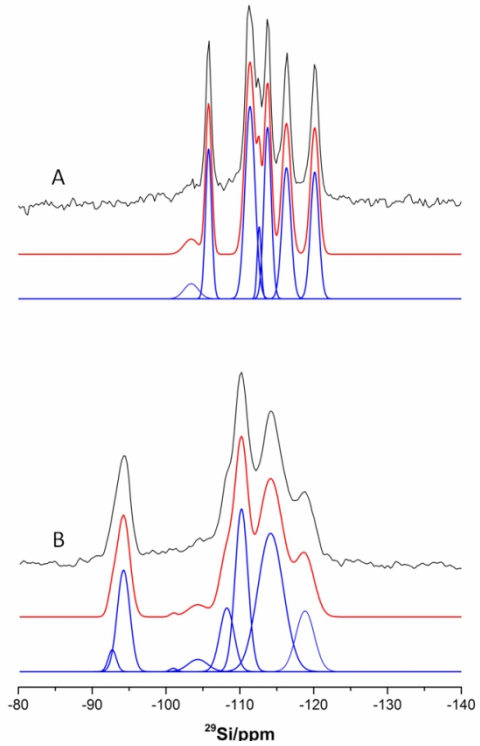

Figure 5. ^{29}Si MAS NMR spectra of calcined (A) and as-made (B) pure silica MWW. In each case, the black curve is the experimental spectrum (top), the red curve is the simulated spectrum (middle) and the blue ones are the deconvoluted components (bottom).

Table 3. Assignment of ^{29}Si MAS NMR resonances for as-made and calcined pure silica MWW synthesized with 10BDMI in fluoride medium[a].

as-made MWW				calcined MWW		
δ	*I*	assignment		δ	*I*	assignment
-92.7	2.8	Q^2				

-94.3	12.9	Q^3			
-101.0	0.4	Q^3	-103.4	1.3	Q^3
-104.3	1.6	Q^4	-105.8	12.6	Q^4, Si1
-108.2	8.1	Q^4	-111.4	16.1	Q^4, Si4
-110.2	20.7	Q^4	-112.6	6.0	Q^4
-114.1	17.6	Q^4	-113.8	14.4	Q^4, Si3
-118.8	7.7	Q^4	-116.3	11.0	Q^4, Si2
			-120.1	10.6	Q^4, Si5

[a]Chemical shifts (δ) in ppm from TMS; relative intensities (*I*) normalized to account for 72 Si atoms per unit cell; Si site numbering and population according to reference[2]; $Q^n = Si(OSi)_n(OH)_{(4-n)}$; the low multiplicity sites Si6-Si8 would be severely overlapped and ascribed to the resonance at -112.6 and its surroundings.

The ^{1}H MAS NMR spectrum of as-made 10BDMI-MWW (Figure 4) shows broad resonances close to the expected region of 10BDMI, while severely overlapped. The spectrum reveals SiOH defects in the as-made zeolite as indicated by a broad resonance around 10 ppm, assigned to SiOH participating in relatively strong hydrogen bonds to charge compensating SiO^- groups.[21] This kind of ^{1}H signal is typically observed in layered precursors to zeolites[19] as well as in high silica zeolites containing large concentrations of connectivity defects.[22]

The ^{29}Si MAS NMR spectra of calcined and as-made pure-silica MWW are shown in Figure 5. The spectra obtained coincide with those of ITQ-1, the first pure silica analogue of MCM-22 and SSZ-25 that we reported years ago.[9-10] According to our previous study, ITQ-1 was successfully synthesized in two different gel systems: one in the presence of N,N,N-trimethyl-1-adamantammonium hydroxide ($TMAda^+OH^-$),[10] hexamethyleneimine (HMI) and Na^+; and the other with $TMAda^+OH^-$ only.[9] For convenience, we denote the samples obtained from those two systems as ITQ-1(Na) and ITQ-1(OH), respectively.

The spectrum of as-made MWW (Figure 5B) is quite similar to those previously reported,[9-10] with minor differences in the resolution of resonances. The characteristic intense resonance at around -94 ppm, which was also observed in ITQ-1(Na) and ITQ-1(OH), is indicative of Si(3Si, 1OH) in the layered MWW precursor. The total concentration of Si-OH connectivity defects here (22.4%Q^3+Q^2, or around 16 Si per unit cell) is considerably lower than those in ITQ-1(Na) (33%) and ITQ-1(OH) (29.2%) but well over the amount needed to end the mww layers (4 SiOH or SiO- per cell, i.e. 5.6%). The decrease in the concentration of connectivity defects here may be, to our assumption, due to the fluoride route.[12a]

Upon calcination at 600 °C, dehydroxylation of silanols occurred and a spectrum with high resolution was achieved, though a small concentration of residual defects (1.8%) was still detected (Table 3), as it was also the case for calcined ITQ-1(OH) (6.9%) but not for the calcined ITQ-1(Na). The ^{29}Si MAS NMR spectrum of the pure silica MWW presented here has 6 much better resolved resonances of Si(4Si) sites with high intensities, resembling more ITQ-1(Na), although the resolution of crystallographic sites was higher in ITQ-1(Na). A tentative assignment of several resonances was made following the way reported for ITQ-1(Na), as shown in Table 3. Considering overlapping of resonances, the spectrum is in reasonable good agreement with the reported structure of MWW, in which there are five crystallographic sites (sites Si1 to Si5) with a multiplicity of 12 and three (Si6, Si7 and Si8) with a multiplicity of 4.[2]

An intriguingly interesting ^{19}F MAS NMR spectrum of the as-made MWW zeolite was obtained, as shown in Figure 6. Four major resonances were detected: the two resonances centered at around -123 ppm and -127 ppm can be assigned to impurities (possibly F bonded to penta or hexacoordinated Si on the outer surface of the crystallites); and the other two resonances are observed at -71 ppm and -83 ppm, with almost the same intensity (relative intensity is 1 to 1.2, respectively), while the low field signal (-71 ppm) is narrower than the high field one (-83 ppm). Because of their chemical shifts, these two resonances likely correspond to “zeolitic fluoride”, i.e. fluoride occluded in small cavities of silica zeolites.[23] We speculate that fluoride may be occluded either in the [$4^1$$5^2$$6^2$] cavities of the MWW framework, which are topologically identical to the ones in which fluoride resides in MFI, or in [$4^2$$6^2$] cavities, where fluoride has

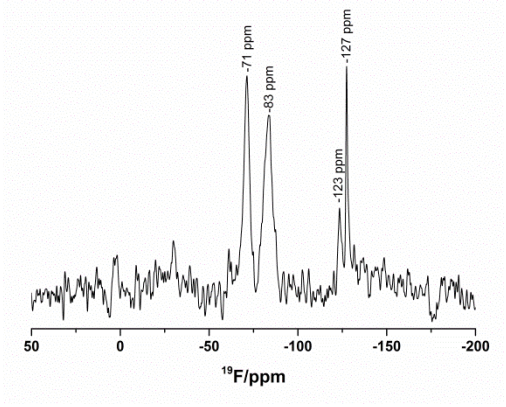

Figure 6. ^{19}F MAS NMR spectrum of the as-made 10BDMI-MWW.

been observed in the CHA framework.[24] The ^{19}F chemical shifts in our pMWW sample (-71, -83 ppm) are close to those observed in MFI samples synthesized with several different imidazolium-based dications (displaying signals ranging from -65 to -70 and from -78 to -80 ppm)[25] as well as in CHA (-64 ppm).[24] The occurrence of these signals will be discussed below based on a computational DFT study.

Figure 7. FTIR spectra of as-made (bottom) and calcined (top) MWW zeolites.

Thus, in 10BDMI-MWW around 6.4 positive charges per unit cell contributed by the dications (3.2 10BDMI cations, as determined by CHN analysis, Table 2) are balanced by both

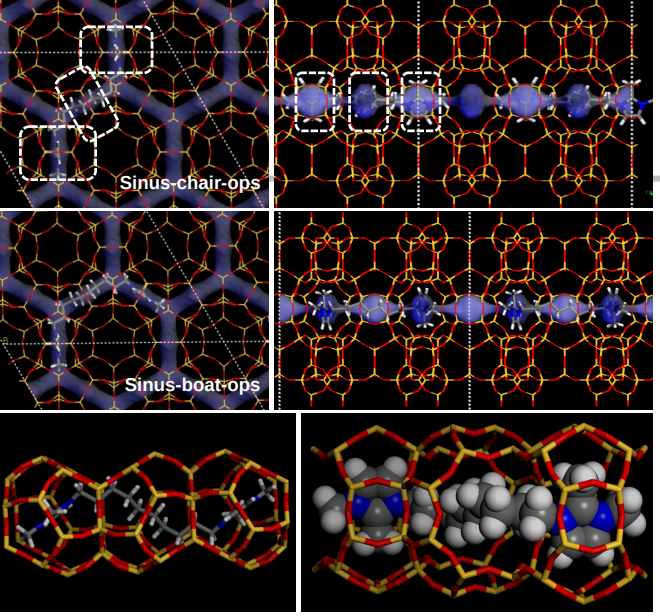

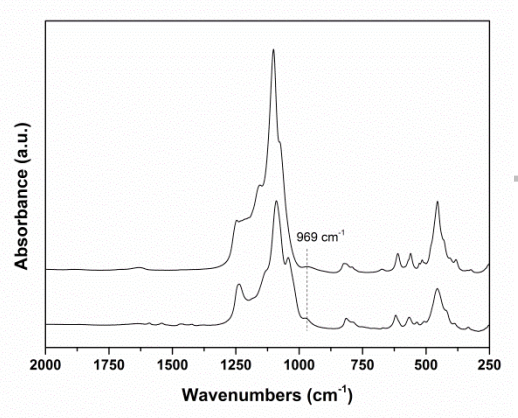

SiO^- groups and occluded fluoride. SiO^- groups are both "structural" Q^3 in the interlayer space (two per cell in two hydrogen bonded SiO^-••••HOSi pairs holding the layers together) and standard "defects" elsewhere. According to the ^{29}Si MAS NMR spectrum of the as-made sample (Figure 5B and Table 3), there are 13.3 Q^3 sites per cell. Four of them must be structural, i.e., the two pairs of SiOH•••−OSi groups holding the layers together. The remaining over 9.3 defects are assigned to connectivity defects that typically occur in groups of one SiO^- and 3 SiOH, thus outnumbering the positive charges by a factor of around 4.[21] If this is so, here charge balance may be achieved by 2 structural silanolates in the interlayer, around 2.3 defective silanolates elsewhere and around 2 fluorides per cell.

After calcination of MWW in air at 600 °C for 5 h, N_2 sorption experiments were performed (Figure S5). The obtained isotherm is type I according to the classification of IUPAC.[26] However, there is an abrupt uptake at P/P0 > 0.8, caused by the presence of mesopores between aggregated crystals. The textural properties of calcined MWW are summarized in Table S1. The pure silica MWW has comparable micropore volume (0.20 cm^3/g) to the reported hydroxide-derived pure silica and aluminosilicate samples, such as ITQ-1 (0.17 cm^3/g) and MCM-22 (0.20-0.28 cm^3/g).[9, 18] The BET surface area is close, though slightly larger, to the reported value for pure silica MWW synthesized in hydroxide medium. The median pore width is 5.6 Å and the maximum pore width is 5.8 Å, obtained from the Horvath-Kawazoe pore size distribution curve, which are above the size range confined by the 10-membered rings in the MWW framework (4.0 × 5.5 Å, the straight 10-ring between layers; 4.1 × 5.1 Å, the sinusoidal 10-ring within the layers). The small discrepancy could be due to the limitations of the method and to the presence of large cavities which, in our experience, tend to result in an overestimation of the pore size.

The FTIR spectra of calcined MWW (Figure 7, top) showed overall bands with higher intensity than those of the as-made sample (Figure 7, bottom) in the region between 250 cm^{-1} and 1350 cm^{-1}, except for a band around 969 cm^{-1}, whose intensity was weakened for the calcined sample compared to its as-made counterpart. This band is typically associated to the stretching vibration of Si-O polarized bonds,[19-20] thus, here we assign this band to the stretching vibration of Si-OH or $Si-O^-$ defects in MWW.[27] The weakening of this band was due to the condensation caused by calcination, which is in agreement with the ^{29}Si MAS NMR spectra.

A long-scan XRD pattern of as-made MWW was indexed using N-TREOR[28] under Expo2004[29] within space group P6/mmm and with unit cell parameters a = 14.186 Å, c = 27.511 Å (Figure S6). The size of the 'c' parameter exceeds by 2.566 Å that of the calcined ITQ-1 material.

Computational results

Molecular mechanics results: location of 10BDMI cations

The MWW framework structure contains two non-intersecting 10-ring channel systems: a) a 2D 10-ring sinusoidal intralayer channel system (within the mww layers), formed by fused small cavities, and b) a 2D 10-ring channel system crossing at the large MWW cup cavities, which corresponds to the interlayer region where the framework is not fully-condensed in the as-synthesized layered precursor (Figure S7). We first studied the location of the 10BDMI cations in this pMWW zeolite system through molecular mechanics models. Since the two channel systems are not interconnected, the occlusion of the 10BDMI dications can be studied independently.

A) Location of 10BDMI cations within the intralayer sinusoidal channels.

The study of different starting configurations for the 10BDMI dications allowed us to find two stable configurations in this channel system, with the dications spanning three adjacent fused cavities of the sinusoidal channel system; a detail of the cavities of the sinusoidal channels is shown in Figure S8: there are three of these cavities per MWW unit cell.

In the first stable configuration, the 10BDMI dications arrange in a 'chair'-like conformation (Figure 8-top), and in the second, they arrange in a 'boat'-like conformation (Figure 8-middle). In addition, the two imidazolium rings of the dication can be oriented towards the same ('ss') or opposite sides ('ops'). Energy results for all these arrangements are reported in Table 4 (energies are expressed in kcal/mol of SDA), and the most stable configurations are displayed in Figure 8.

Table 4. Interaction energies of the 10BDMI dications located in the sinusoidal channels and in the interlayer system.

Channel	Config.	Conform.	Interaction Energy
Sinusoidal	Chair	ss	-91.0
		ops	-89.6
	Boat	ss	-88.4
		ops	-87.5
Interlayer	Cup cages	ss	-66.4
		ops	-64.8
	Interlayer space	ops	-49.2

It can be clearly observed that the 10BDMI dication has the appropriate molecular size as to fit nicely within the sinusoidal channels, spanning three consecutive cavities (either in 'chair' or

'boat' configuration), with two of the cavities filled by the imidazolium rings and the other one filled by the alkyl spacer (see Figure 8). Both ('chair' or 'boat') configurations are similarly stable, though the 'chair' is slightly more favourable. On the other hand, both 'ss' and 'ops' conformations have very similar stabilities (Table 4). As there are three of these cavities per MWW u.c., this will account for one 10BDMI dication per MWW u.c. in the sinusoidal channels (spanning cavities of adjacent unit cells). If we look in detail at the location of the dications within this system (Figure 8-bottom), a clear geometrical relationship is directly established: the dimethylimidazolium rings fit nicely within the intralayer cavities (right), and hence should be good directors of this structural unit. On the other hand, the 10C spacer has the appropriate size to connect two cavities at the right distance as to allow for the formation of the sinusoidal channels building up the mww layers, showing a very good geometric fitting. Hence, we conclude that 10BDMI dications are very efficient for promoting the crystallization of the mww layers through filling the void space and ordering the intralayer sinusoidal channels.

B) Location of 10BDMI cations within the interlayer space.

We next studied how these mww layers would connect to each other in the presence of 10BDMI. With this purpose, we analyzed the incorporation of 10BDMI in the interlayer space of the pMWW framework, which contains the large MWW cup cages (still as two unconnected halves in the as-made state) as well as what in the calcined state would be 10-R channels (Figure S7, interlayer channel); we emphasize again that the layers are not fully-condensed yet.

After a first set of calculations, we found two stable configurations for 10BDMI in the interlayer region. In the first location ('cup cages' in Table 4), the half-cages in the interlayer region are occupied by imidazolium rings, and the mww layers are then connected through the alkyl spacer of 10BDMI (see Figure 9-top). Again we see that the 10C spacer has the appropriate length as to allow for the connection between the layers, allowing them to site at the appropriate distance as to establish H-bond interactions between the layers. In the other configuration ('interlayer' in Table 4), the organic cations locate in the interlayer space, parallel to the 'ab' planes of the layer (Figure 9-bottom), this position developing lower interaction. However, because of space-filling issues and considering the overall SDA content (see discussion below), we deem likely that both cup cavities and interlayer space should be filled by the imidazolium rings. By looking at the interaction energies, we conclude that the space-filling ability of the dication in the different topological units of the MWW framework follows the order: sinusoidal channels > cups > interlayer space, probably due to a decreasing confinement effect going from intralayer to interlayer space.

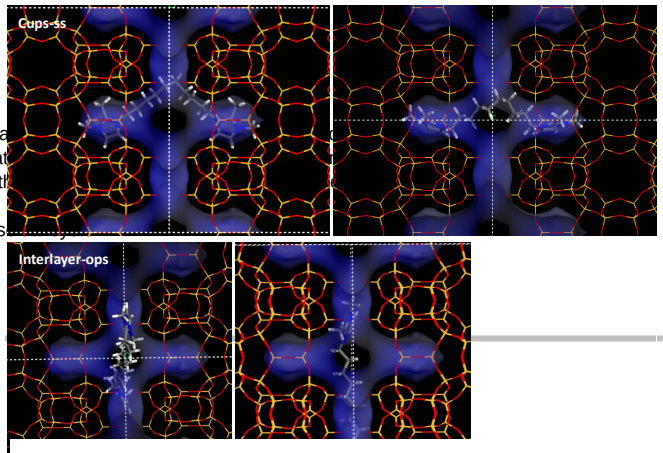

Figure 8. Loca
(top) or 'boat
highlighted wit
relationship of
intralayer sinus

Figure 9. Location of 10BDMI dications in the interlayer space, with imidazolium rings in the cup cages (top, two orientations) or parallel to the layers in the interlayer region (bottom, three orientations).

Given the experimental packing value found of 3.2 SDAs/u.c., 10BDMI dications should locate both in the cup cages and in the interlayer space, in addition to one SDA/u.c. in the sinusoidal channel system. Indeed, the larger space of the interlayer region caused by the non-condensation of the mww layers gives enough room as to host simultaneously 10BDMI dications in the cups and in the interlayer region, possibly stabilized by hydrophobic interactions between the apolar alkyl spacers of the two dications. Because of the great flexibility provided by the alkyl chain, it could also occur that 10BDMI cations site one imidazolium ring in the cup and the other in the interlayer region. In sum, the structure-directing role of 10BDMI towards the crystallization of layered pMWW seems to be a consequence of the good fit between the imidazolium rings and the cavities of the intralayer sinusoidal channels and the half-cages of the interlayer space. On the other hand, the 10C spacer has the appropriate length and flexibility as to spatially order and connect these topological units, both the intralayer cavities as well as the interlayer cups, at the right distance and orientation to promote the crystallization of the pMWW framework.

DFT results

After gaining insight on the host-guest chemistry of the 10BDMI-pMWW system by molecular mechanics models, we tried to unravel by DFT methods the particular ^{19}F and ^{13}C NMR features observed experimentally. We first studied the stability of F hosted within the [$4^1 5^2 6^2$] (bonded to T1, T2, T4, T5, T7 or T8) or the [$4^6 6^2$] (D6R, bonded to T3) cavities (Figure 10-top) in the absence of organic cations; the location for F in the smaller [4^3] cages, bonded to T6, was very unstable. This should give an idea of the intrinsic stability of the different positions for F, from a topological point of view. The relative stability of the different positions for F, as well as the theoretical ^{19}F NMR chemical shifts calculated, are reported in Table 5; Figure 10 (bottom) shows the geometry-optimized structures of F attached to the different T sites. The relative energies (given in kcal/mol per MWW u.c.) indicate that the most stable position for F (from a topological point of view, without taking into account the interaction with the organic SDA cations) is T3 (Table 5), i.e. in the D6R (Figure 10-T3), giving a ^{19}F NMR theoretical signal at ~-68 ppm, which is close to the experimental value observed at -71 ppm. The next most stable position for F is bonded to T7 (with a relative energy of 2.5 kcal/mol), with F locating quite in the middle of the [$4^1 5^2 6^2$] cavity (Figure 10-T7); F in this position should give a theoretical NMR signal at ~-93 ppm. The next most stable position for F in the [$4^1 5^2 6^2$] cavities is T5 (with a relative energy of 6.7 kcal/mol), where F is bonded to the 4-ring (Figure 10-T5), giving a theoretical ^{19}F NMR signal at -79 ppm, close to the other signal observed experimentally (at -83 ppm). The rest of positions for F in the [$4^1 5^2 6^2$] cavities are less stable (by more than 9 kcal/mol, with a stability order of T4 > T8 > T2 > T1) (Table 5). If we compare with the experimental ^{19}F NMR spectrum of our real material, these results suggest that, without considering the effect of the SDA organic cations, the two ^{19}F NMR signals observed could be tentatively assigned to F in the D6Rs (bonded to T3), giving the signal at -71 ppm, and in the [$4^1 5^2 6^2$] cavities attached to T5, giving the signal at -83 ppm.

Table 5. Relative energy (R.E., in kcal/mol per MWW u.c.) and theoretical ^{19}F NMR chemical shift (^{19}F δ, in ppm) calculated in the absence of organic cations (no SDA) for F bonded to the different T positions. Last column

displays the theoretical ^{19}F NMR chemical shift calculated in the presence of the SDA cations; averaged values between all the different relative orientations are given.

We next studied the different systems (excluding the least stable T1 and T2 positions for F), but this time including 1-pentyl-2,3-dimethylimidazolium (5DMI) organic cations (as a representation of the 10BDMI cations, as explained in the computational details); they were located both in the sinusoidal intralayer channels and in the cups of the interlayer region. Different relative orientations of F and the 5DMI organic cations (by 180º rotation of the imidazolium plane) were studied (see Figure S9); relative energy results and theoretical ^{19}F NMR signals are reported in Table S2, and averaged (between all the different orientations studied) ^{19}F δ values for each T position are reported in Table 6 (right column, SDA).

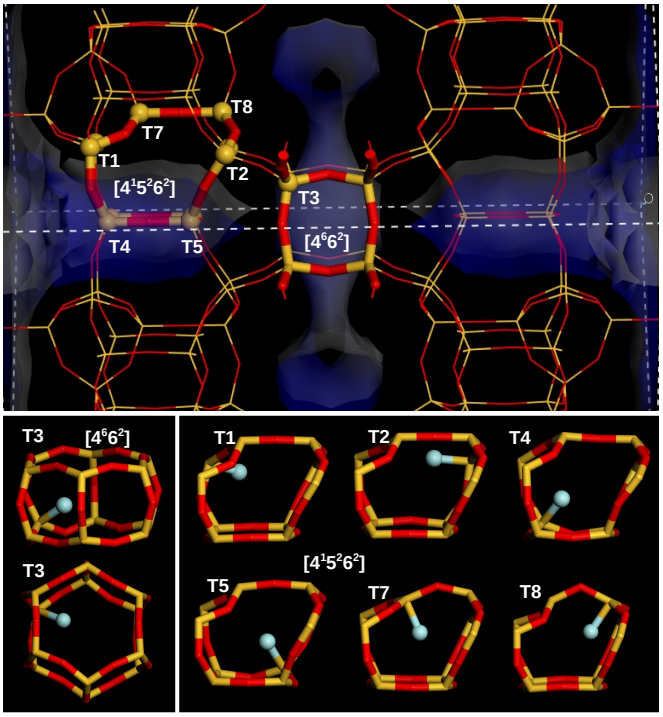

Figure 10. Different positions (after geometry optimization in the absence of organic SDA cations) of F inside the [4^{6}6^2] (bottom-left: T3) or [4^{1}5^{2}6^2] (bottom-right, bonded to the different T positions: T1, T2, T4, T5, T7 or T8) cavities.

Energy results (Table S2) show that, in general, the most stable location for F in the presence of 5DMI cations corresponds to T3, within the D6Rs, as was the case in the absence of SDAs. However, we note that, depending on the orientation of the SDAs and F, very different energies are obtained. The ^{19}F NMR signals for F in this position ranges between -61 and -71 ppm depending on the particular orientation, with an average value at -65 ppm (Table 5). Hence, still we could tentatively assign the experimental signal at -71 ppm to F in the D6Rs.

We next studied F located within the [4^{1}5^{2}6^2] cavities, bonded to T4, T5, T7 or T8 (Table S2). First we observe that the relative energies for F bonded to T4 are rather high (at least by more than 22 kcal/mol per MWW u.c.), suggesting a low stability, which was also observed in the absence of cations (Table 5). Moreover, the ^{19}F NMR theoretical signal for this position ranges from -47 to -62 ppm (except for a single case at -65 ppm), with an average value at -53 ppm, which is far from the experimentally observed signals. In the same line, although some orientations are not so unfavorable for F in T8 (Table S2),

F site	F location	R.E. (no SDA)	^{19}F δ (no SDA)	$^{19}F_{av}$ δ (SDA)
T1	[4¹5²6²]	14.2	-104.0	---
T2	[4¹5²6²]	14.9	-80.3	---
T4	[4¹5²6²]	9.5	-61.4	-53.4
T5	[4¹5²6²]	6.7	-79.4	-74.7
T7	[4¹5²6²]	2.5	-93.3	-76.0
T8	[4¹5²6²]	10.5	-61.8	-60.1
T3	[4⁶6²]	0.0	-68.1	-65.1

however the theoretical values are close to -60 ppm, again far from the experimental values. Hence we tentatively discard these two positions.

In the case of F bonded to T5, ^{19}F NMR signals are found between -68 and -82 ppm, with an average value at -75 ppm (Table 5). Similarly, F bonded to T7 in the [4¹5²6²] cavities would give signals between -74 and -78 ppm, with an average value at -76 ppm.

Taking into account all the theoretical ^{19}F NMR signals as a function of the T position and 5DMI orientation and comparing with the experimental signals, we tentatively assign the band at -71 ppm to F occluded in the D6Rs, bonded to T3, and the signal at -83 ppm with F occluded within the [4¹5²6²] cavities, bonded probably to T5 or T7; both cavities have been previously found to host F anions.[22, 24, 30] In any case, we note that the relative stability of the final host-guest zeolite-SDA system (as calculated in Table S2) might not impose the location for F in the final material since F will become part of [4¹5²6²] or D6R cavities already during the nucleation/crystallization process when the zeolite has not yet been formed, and hence the SDA might not impose the location of F but instead could be controlled by kinetic factors. On the other hand, we have also found that the ^{19}F NMR signal for T5 is strongly dependent on the orientation of the imidazolium rings, and indeed signals around -71 and -82 ppm have been found for F bonded to T5, depending on the particular 5DMI/F orientation; hence we cannot unambiguously discard this to be the origin for the experimental spectrum. Moreover, since no Si-F signal is observed in the ^{29}Si NMR spectrum, it is possible that F might be jumping between different positions, what also could affect the experimental NMR band. Therefore, it is difficult to establish with certainty which of the two options corresponds to the actual case.

We finally analyzed the origin for the splitting of the ^{13}C NMR signal at 10 ppm observed experimentally (Figure 3, C_e). Table 6 reports the theoretical ^{13}C NMR signals for the C atoms of the imidazolium rings of the 5DMI cations located in the sinusoidal channels, 'sinus', and in the cups of the interlayer region, 'interl', for F bonded to different T positions. On the one hand, we clearly observe that the signal corresponding to methyl C_e is dependent on the location of the imidazolium ring: if it is in cavities of the sinusoidal channels, this gives a ^{13}C resonance at around 12-14 ppm, whereas if it is in the cups of the interlayer region, this gives a signal at around 8-9 ppm. The occurrence of these two NMR signals for C_e is consistently repeated in all the systems, regardless of the 5DMI relative orientation or of the F

position (Table 6). The presence of these two signals is in reasonable agreement with the experimental splitting of this NMR resonance at 8.8 and 10.4 ppm, suggesting that the occurrence of the two peaks is a consequence of the two types of locations for the imidazolium rings of the SDA dications, in the cavities of the sinusoidal channels and in the cups of the interlayer region. This might be associated to the higher confinement of the imidazolium rings hosted in the cavities of the sinusoidal channels compared to that in the cups (as suggested by the higher interactions, see Table 4), which is mostly manifested in the C_e methyl groups. If we look through the theoretical ^{13}C NMR data (Table 6), we also find a recurrent difference in the chemical shift of C_d, with two resonances at 37-38 and 40-43 ppm, but these are not distinguished in the experimental spectrum (only one signal is observed, Figure 3). This discrepancy might come from artifacts due to the approximations made in our model, where we use the more mobile 5DMI cations (rather than 10BDMI) as well as fully-condensed periodic MWW frameworks.

Table 6. Examples of theoretical ^{19}F and ^{13}C NMR chemical shifts (in ppm) for systems with F bonded to T3, T5 and T7. 4 5BDMI cations per MWW u.c. are included, two in the interlayer region and two in the sinusoidal channels. Labels of the C atoms are the same as in Figure 3.

F site	F NMR	C NMR	Ce	Cd	Cf	Cc	Cb	Ca
T3	-71.3	interl1	8.0	38.4	53.7	125.9	126.5	144.2
		interl2	8.5	37.9	54.4	125.8	125.1	145.3
		sinus1	12.0	42.7	58.5	128.1	124.2	146.2
		sinus2	12.0	41.8	54.2	128.0	124.6	141.6
T5	-80.9	interl1	9.5	37.4	53.7	126.2	124.8	146.4
		interl2	8.8	36.6	55.0	126.4	124.7	145.4
		sinus1	14.2	41.0	54.5	131.1	124.0	141.2
		sinus2	14.7	41.4	56.7	126.2	123.6	148.9
T7	-75.5	interl1	8.8	37.0	53.7	126.9	124.5	145.6
		interl2	9.3	36.6	55.1	127.3	124.1	145.2
		sinus1	13.6	42.0	54.6	128.6	125.4	143.2
		sinus2	13.3	40.4	59.6	129.1	123.4	150.1

Conclusions

As the length of the spacer between 1,2-dimethylimidazolium moieties increases beyond six methylene units, the specific structure direction of this kind of dications towards pure silica zeolites shifts from STW (in which they cannot fit) towards either *BEA (for eight methylene units) or MWW (for ten methylene units). In all the cases (n=4, 5, 6, 8, 10) when specificity is lost (i.e., upon decreasing concentration or increasing temperature or in any case for n= 5, 6) the default structure that crystallizes is MTW. It is interesting to note that the default structure is a denser zeolite with a one-dimensional system of pores, while the metastable zeolites requiring a higher specificity contain a multidimensional channel system featuring large cavities or pore-crossings, thus affording a larger organic content.

The synthesis of pure silica MWW presented here is the first case of synthesis of this material in fluoride media without using Al, B or alkali cations. We note that in the presence of alkali cations and/or Al or B, the effective concentration of fluoride able to interact with silicon shall diminish, since the solubility of NaF and KF is not high and fluoride has also a tendency to strongly bind to Al and B. However, and despite the “genuine” character of our fluoride route to MWW, charge balance is achieved not only by occluded fluoride, but also by “structural” $Si\text{-}O^-$ groups in the interlayer region, involved in relatively strong hydrogen bonds with Si-OH groups in the adjacent layer, and “defect” SiO^- elsewhere. Although the as-made material synthesized here does contain fewer defects than those prepared by the hydroxide route, its amount still exceeds that strictly needed to maintain the layers and balance the SDA charges.

Based on molecular mechanics simulations, we propose a model in which the long 10BDMI dication directs the formation of the layers thanks to its good fitting and interaction inside the two dimensional intralayer sinusoidal channels. Additionally, the dication helps keep the layers together by its proper fitting inside the large half-cups, while affording the formation of layer-to-layer hydrogen bonds. On the other hand, based on DFT calculations, fluoride is proposed to reside in the $[4^15^26^2]$ and $[4^66^2]$ cages of the MWW structure. DFT calculations also explain the splitting of a ^{13}C resonance as due to the two different location sites of the organic dication: with the imidazolium rings confined in the half-cups of the interlayer region and within the cavities of the sinusoidal channels, providing different confinement effects.

Experimental Section

Synthesis of the organic structure-directing agents

The organic SDAs used in this work are imidazolium-based long dications, which are built by using a linear methylene chain as a spacer with 8 or 10 carbons connecting 1,2-dimethylimidazolium charged moieties at both ends. The two kinds of dications are denoted as 8BDMI and 10BDMI, respectively. Synthesis of the dications started by dissolving 0.14 mol of 1,2-dimethylimidazole (Sigma-Aldrich, 98%) in a flask containing chloroform (50 mL) (Sigma-Aldrich, 99%), then 0.07 mol of linear dibromo-alkane (Sigma-Aldrich, 98% for n=8, and 97% for n = 10) was added together with another dosage of chloroform (50 mL). The resulting mixture was kept stirring magnetically and refluxed for 4 days. The thick transparent oily product was finally obtained after rotoevaporation to remove the solvent. The SDAs were analyzed by dissolving the bromides in D_2O and the corresponding ^1H and ^{13}C NMR spectra were recorded (Figure S10 and S11), confirming the acceptable purity of 8BDMI and 10BDMI. The hydroxide forms of the dications were obtained by anion exchange of the corresponding bromides using 550A (OH) resin (Sigma-Aldrich, 1.1 mequiv./1 mL). The detailed ion-exchange procedure can be found in a previous work.[25] The hydroxide solution was concentrated by rotoevaporation and its final concentration was determined by titration using phenolphthalein as indicator.

Synthesis of zeolites

A general synthesis protocol was as follows. First, tetraethylorthosilicate (TEOS, 98%, Sigma-Aldrich) was hydrolyzed at room temperature in the hydroxide aqueous solution of the SDA. All the ethanol produced together with some water was evaporated to reach the desired composition (monitored by weight). Then, hydrofluoric acid (HF, Sigma-Aldrich, 48%) was added with a pipette (*Cautious! Operation must be done in the fume hood*) and the resulting mixture was kneaded exhaustively using a spatula by hand. The final gel composition was 1 SiO_2: 0.25 $R(OH)_2$: 0.5 HF: x H_2O, where x = 3, 4 and 5 and R stands for the dications. The thick or powdery gel, depending on the water content, was divided into Teflon lined stainless steel autoclaves, which were heated under rotation at different temperatures. The autoclaves were

taken out from the oven at different time intervals and the solid product was washed with sufficient amount of demineralized water and dried at 100 °C. The as-made samples were calcined in a muffle at 600 °C for 5 h in order to remove the occluded organics.

Characterization

Powder X-ray diffraction (PXRD) was used to identify the recovered solids. The diffraction patterns were obtained in a Bruker D8 Advance diffractometer using Cu Kα radiation (λ = 1.5418 Å). For indexing as-made pMWW, long scan data were also obtained. The amount of organic matter occluded in the as-made zeolites was determined by CHN elemental analysis using a LECO CHNS-932 analyzer. Thermal gravimetric analysis was carried out in a SDT Q600 TA instrument under air flow (100 ml/min) heating from 25 °C to 1000 °C (with a heating rate of 10 °C/min). The morphologies of the obtained samples were investigated by field emission scanning electron microscopy (FE-SEM), using a Philips XL30 S-FEG. Multinuclear magic angle spinning (MAS) NMR spectroscopy of as-synthesized samples was obtained at room temperature on a Bruker AV-400-WB equipment and the details can be found in our previously reported work.[31] Fourier Transform infrared spectra were obtained with a Bruker IFS 66/S spectrophotometer. Nitrogen adsorption/desorption were carried out in a Micromeritics ASAP 2010 equipment at the N_2 liquefaction temperature of 77 K. The calcined samples were outgassed under vacuum at 120 °C.

Computational details

Molecular mechanics simulations were performed in order to find the location of 10BDMI within the pMWW framework; simulations were carried out using the Forcite module implemented in Materials Studio.[32] The pMWW structure was modelled by altering the MWW topology according to the 'c' unit cell parameter determined by indexing of the XRD pattern (27.51 Å), in order to account for the layered nature of the pMWW framework observed experimentally. O atoms were added in all the terminal positions (between layers). The geometry of this layered structure was kept fixed during the force-field calculations. Molecular structures and the interaction energies of the organic SDA dications with the framework were described with the CVFF forcefield.[33]

Due to the large size of the SDA cations, 2 × 2 × 1 MWW supercells have been used as zeolite models. The 10BDMI cations were manually docked in the framework in the required position/orientation; unless specified, 1 SDA per supercell was studied. The most stable location was obtained by simulated annealing calculations. The interaction energy was calculated by subtracting the energy of the dications in vacuo to the total energy of the system; all the energy values are given in kcal/mol.

We also performed DFT+D calculations, and calculated theoretically the F and C chemical shieldings as a function of its position and of the orientation of the organic cations. As mentioned for the molecular mechanics model, the large size of the 10BDMI cations requires MWW supercells to be hosted, preventing the use of DFT with these large systems. Hence, we used smaller cations which correspond to half the 10BDMI dications, i.e. 1-pentyl-2,3-dimethylimidazolium (5DMI), which allowed for the use of single MWW unit cells as zeolite model large enough to host them, two on each location, for a total of 4 5BDMI cations per MWW u.c.. This made the system accessible to a thorough computational study by DFT+D; moreover, we found that the location of these monocations, with the imidazolium rings siting in the cups of the interlayer region and in the cavities of the sinusoidal channels, properly resembled the location of the original 10BDMI dications, especially regarding features related with the F position and interaction with the imidazolium rings, and hence with the ^{19}F and ^{13}C NMR features. In the same line, we used fully-condensed MWW frameworks[2] in order to simplify the DFT calculations since the layered nature of our MWW framework should not affect the orientation of the imidazolium rings, neither the F location in the selected position. F bonded to all the different positions were studied, residing in the $[4^1 5^2 6^2]$, $[4^6 6^2]$ and $[4^3]$ cavities of the MWW framework (the last case was found to be very unstable, and hence was discarded). The 5DMI cations were loaded with the imidazolium ring in the same position as the ones found for 10BDMI in the previous molecular mechanics study. Different relative orientations of F and the 5DMI cations in both locations (in the intralayer cavities and in the cups of the interlayer region) were studied, two on each location, for a total of 4 5BDMI cations per MWW u.c.. The different systems were geometry optimized at the DFT+D level, which were performed using plane-waves as basis set (with a cut-off of 571.4 eV), and the PBE generalized gradient approximation,[34] as implemented in the CASTEP module[35] in Materials Studio.[32] The stability of the different systems was determined by calculating the relative energies (R.E.), referring to the most stable case; these are given in kcal/mol per MWW unit cell. Calculation of the NMR parameters were performed with the gauge-including projector augmented-wave method (GIPAW) developed by Pickard and Mauri.[36] The chemical shift for a nucleus in a given position (δ(r)) is calculated as:

$$\delta(r) = \sigma_{ref} - \sigma(r)$$

where σ(r) is the isotropic shielding obtained from the calculations. In order to compare with the experimental ^{19}F and ^{13}C chemical shifts, we chose σ_{ref} values of 137 and 174 ppm, respectively, the same as in our previous works,[16, 22] so that the theoretical and experimental chemical shifts roughly coincide.

Acknowledgements

Financial support provided by the Spanish Ministry of Economy and Competitiveness (projects MAT2015-71117-R and MAT2016-77496-R) is acknowledged. P. L. is grateful to the China Scholarship Council (CSC) for a fellowship and to the Dalian Institute of Chemical Physics for permission to leave. Centro Técnico Informático-CSIC is acknowledged for running the calculations, and Biovia is acknowledged for providing the computational software.

Keywords: MWW zeolite • fluoride media • structure-direction • molecular mechanics • DFT calculation

[1] M. E. Davis, R. F. Lobo, *Chem. Mater.* **1992**, *4*, 756-768.
[2] http://www.iza-structure.org/databases/accessed on 6/27/2018
[3] E. M. Flanigen, R. L. Patton, U.S. Patent 4,073,865, **1978**.
[4] a) J. L. Guth, H. Kessler, J. M. Higel, J. M. Lamblin, J. Patarin, A. Seive, J. M. Chezeau, R. Wey, in *Zeolite Synthesis, Vol. 398*, American Chemical Society, **1989**, pp. 176-195; b) H. Kessler, J. Patarin, C. Schott-Darie, *Stud. Surf. Sci. Catal.* **1995**, *26*.
[5] L. Puppe, J. Weisser, U.S. Patent 4,439,409, **1984**.
[6] S. I. Zones, U.S. Patent 5,202,014, **1993**.
[7] M. E. Leonowicz, J. A. Lawton, S. L. Lawton, M. K. Rubin, *Science* **1994**, *264*, 1910-1913.
[8] R. Millini, G. Perego, W. O. Parker, G. Bellussi, L. Carluccio, *Microporous Mater.* **1995**, *4*, 221-230.
[9] M. A. Camblor, C. Corell, A. Corma, M.-J. Díaz-Cabañas, S. Nicolopoulos, J. M. González-Calbet, M. Vallet-Regí, *Chem. Mater.* **1996**, *8*, 2415-2417.
[10] M. A. Camblor, A. Corma, M.-J. Díaz-Cabañas, C. Baerlocher, *J. Phys. Chem. B* **1998**, *102*, 44-51.
[11] H. Du, M. Kalyanaraman, M. A. Camblor, D. H. Olson, *Microporous Mesoporous Mater.* **2000**, *40*, 305-312.
[12] a) M. A. Camblor, L. A. Villaescusa, M. J. Díaz-Cabañas, *Top. Catal.* **1999**, *9*, 59-76; b) P. Lu, L. A. Villaescusa, M. A. Camblor, *Chem. Rec.* **2018**, *18*, 1-12.
[13] T. Blasco, M. A. Camblor, A. Corma, P. Esteve, J. M. Guil, A. Martínez, J. A. Perdigón-Melón, S. Valencia, *J. Phys. Chem. B* **1998**, *102*, 75-88.
[14] D. H. Olson, X. Yang, M. A. Camblor, *J. Phys. Chem. B* **2004**, *108*, 11044-11048.
[15] a) S. I. Zones, S.-J. Hwang, *Microporous Mesoporous Mater.* **2011**, *146*, 48-56; b) R. Aiello, F. Crea, F. Testa, G. Demortier, P. Lentz, M. Wiame, J. B. Nagy, *Microporous Mesoporous Mater.* **2000**, *35-36*, 585-595.

[16] P. Lu, L. Gomez-Hortiguela, L. Xu, M. A. Camblor, *J. Mater. Chem. A* **2018**, *6*, 1485-1495.

[17] M. A. Camblor, S.B. Hong, in *Porous Materials* (Ed.: D. W. Bruce, D. O'Hare, R. I. Walton), Willey, **2011**, pp. 265-32**5**.

[18] a) M. Cheng, D. Tan, X. Liu, X. Han, X. Bao, L. Lin, *Microporous Mesoporous Mater.* **2001**, *42*, 307-316; b) L. Liu, M. Cheng, D. Ma, G. Hu, X. Pan, X. Bao, *Microporous Mesoporous Mater.* **2006**, *94*, 304-312.

[19] A. Rojas, M. A. Camblor, *Chem. Mater.* **2014**, *26*, 1161-1169.

[20] D. Scarano, A. Zecchina, S. Bordiga, F. Geobaldo, G. Spoto, G. Petrini, G. Leofanti, M. Padovan, G. Tozzola, *J. Chem. Soc., Faraday Trans.* **1993**, *89*, 4123-4130.

[21] H. Koller, R. F. Lobo, S. L. Burkett, M. E. Davis, *J. Phys. Chem.* **1995**, *99*, 12588-12596.

[22] A. Rojas, L. Gomez-Hortiguela, M. A. Camblor, *J. Am. Chem. Soc.* **2012**, *134*, 3845-3856.

[23] M. A. Camblor, P. A. Barrett, M. a.-J. Díaz-Cabañas, L. A. Villaescusa, M. Puche, T. Boix, E. Pérez, H. Koller, *Microporous Mesoporous Mater.* **2001**, *48*, 11-22.

[24] L. A. Villaescusa, I. Bull, P. S. Wheatley, P. Lightfoot, R. E. Morris, *J. Mater. Chem.* **2003**, *13*, 1978-1982.

[25] P. Lu, L. Gomez-Hortiguela, M. A. Camblor, *Dalton Transactions* **2018**, *47*, 7498-7504.

[26] K. S. W. Sing, *Pure Appl. Chem.***1982**, *54,* 2201-2218.

[27] B. Marler, H. Gies, *Eur. J. Mineral.* **2012**, *24*, 405-428.

[28] A. Altomare, C. Giacovazzo, A. Guagliardi, A. G. G. Moliterni, R. Rizzi, W. P.-E, *J. Appl. Crystallogr.* **2000**, *33*, 1180-1186.

[29] A. Altomare, R. Caliandro, M. Camalli, C. Cuocci, C. Giacovazzo, A. G. G. Moliterni, R. Rizzi, *J. Appl. Crystallogr.* **2004**, *37*, 1025–1028.

[30] H. Koller, A. Wölker, L. A. Villaescusa, M. J. Díaz-Cabañas, S. Valencia, M. A. Camblor, *J. Am. Chem. Soc.* **1999**, *121*, 3368-3376.

[31] A. Rojas, E. Martinez-Morales, C. M. Zicovich-Wilson, M. A. Camblor, *J. Am. Chem. Soc.* **2012**, *134*, 2255-2263.

[32] Forcite and CASTEP modules. BIOVIA Materials Studio 2017 R2.

[33] P. Dauber-Osguthorpe, V. A. Roberts, D. J. Osguthorpe, J. Wolff, M. Genest, A. T. Hagler, *Proteins Struct. Func. Genet.* **1988**, *4*, 31-47.

[34] J. P. Perdew, K. Burke, M. Ernzerhof, *Phys. Rev. Lett.* **1996**, *77*, 3865-3868.

[35] J. Clark Stewart, D. Segall Matthew, J. Pickard Chris, J. Hasnip Phil, I. J. Probert Matt, K. Refson, C. Payne Mike, in *Z.Kristallo. – Cryst. Mater.* **2005**, *220*, 567-570.

[36] a) C. J. Pickard, F. Mauri, *Phys. Rev. B* **2001**, *63*, 245101; b) M. Profeta, F. Mauri, C. J. Pickard, *J. Am. Chem. Soc.* **2003**, *125*, 541-548; c) C. Bonhomme, C. Gervais, F. Babonneau, C. Coelho, F. Pourpoint, T. Azaïs, S. E. Ashbrook, J. M. Griffin, J. R. Yates, F. Mauri, C. J. Pickard, *Chem. Rev.* **2012**, *112*, 5733-5779.